

## RADIONUCLIDE IONIZATION IN PROTOPLANETARY DISKS: CALCULATIONS OF DECAY PRODUCT RADIATIVE TRANSFER

L. ILSEDORE CLEEVES<sup>1</sup>, FRED C. ADAMS<sup>1,2</sup>, EDWIN A. BERGIN<sup>1</sup>, RUUD VISSER<sup>1</sup>

<sup>1</sup>Department of Astronomy, University of Michigan, 500 Church Street, Ann Arbor, MI 48109 and

<sup>2</sup>Department of Physics, University of Michigan, 450 Church Street, Ann Arbor, MI 48109

*Draft version June 8, 2018*

### ABSTRACT

We present simple analytic solutions for the ionization rate  $\zeta_{\text{SLR}}$  arising from the decay of short-lived radionuclides (SLRs) within protoplanetary disks. We solve the radiative transfer problem for the decay products within the disk, and thereby allow for the loss of radiation at low disk surface densities; energy loss becomes important outside  $R \gtrsim 30$  AU for typical disk masses  $M_g = 0.04 M_\odot$ . Previous studies of chemistry/physics in these disks have neglected the impact of ionization by SLRs, and often consider only cosmic rays (CRs), because of the high CR-rate present in the ISM. However, recent work suggests that the flux of CRs present in the circumstellar environment could be substantially reduced by relatively modest stellar winds, resulting in severely modulated CR ionization rates,  $\zeta_{\text{CR}}$ , equal to or substantially below that of SLRs ( $\zeta_{\text{SLR}} \lesssim 10^{-18} \text{ s}^{-1}$ ). We compute the net ionizing particle fluxes and corresponding ionization rates as a function of position within the disk for a variety of disk models. The resulting expressions are especially simple for the case of vertically gaussian disks (frequently assumed in the literature). Finally, we provide a power-law fit to the ionization rate in the midplane as a function of gas disk surface density and time. Depending on location in the disk, the ionization rates by SLRs are typically in the range  $\zeta_{\text{SLR}} \sim (1 - 10) \times 10^{-19} \text{ s}^{-1}$ .

*Subject headings:* accretion, accretion disks — circumstellar matter — radiative transfer — stars: pre-main sequence

### 1. INTRODUCTION

Ionization plays an important role in setting thermal, dynamical, and chemical properties of protoplanetary disks. The dominant ionization processes thought to be active in such disks include photoionization from stellar and interstellar UV and X-ray radiation, thermal ionization, ionization by the decay products of short-lived radionuclides (SLRs), and cosmic ray (CR) ionization (e.g., Glassgold et al. 1997; Finocchi & Gail 1997; Glassgold & Najita 2001; Walsh et al. 2012). Of these sources, only CR and SLR-decay are able to provide ionization in the densest and coldest layers of the disk where UV and X-ray photons are highly attenuated. However, the importance of CR ionization is highly uncertain, and position dependent, due to stellar-wind modulation from the central star (Cleeves et al. 2013, hereafter Paper I). With the substantially reduced CR rates expected for these disk systems, SLR-decay is left as the dominant midplane ionization contributor at distances beyond the hard X-ray dominated region,  $R \gtrsim 10$  AU from the central star.

Indeed, the Solar System’s meteoritic record points to an early enhancement ( $\sim 10$  times the mean ISM abundance; Umebayashi & Nakano 2009) of  $^{26}\text{Al}$ , the most chemically significant of the SLRs, indicating an enrichment of massive star byproducts in the Solar birth cluster (Adams 2010). Furthermore, maps of 1.808 MeV  $\gamma$ -rays resulting from  $^{26}\text{Al}$  decay confirm an enhancement of SLRs near major star-forming regions (Diehl et al. 2006). While the ubiquitous presence of SLRs during star-formation and subsequent disk-formation is expected, the degree to which their energetic decay products contribute to the ionization rate remains uncer-

tain. For example, there is inherent time evolution in both the total mass of SLRs (set by their respective half-lives where  $t = 0$  corresponds to the time of formation of CAIs; MacPherson et al. 1995) and the spatial distribution of dust particles that carry the SLRs, which tend to settle towards the midplane with time (Umebayashi et al. 2013). Furthermore, the diversity of original sources of radioactive particles, including supernovae (Cameron & Truran 1977), Wolf-Rayet winds (Arnould et al. 1997; Gaidos et al. 2009), and stellar spallation (Lee et al. 1998; Shang et al. 2000), adds further complexity to characterizing the initial abundances of SLRs present at the time of disk-formation (see also Adams 2010). Nevertheless, the meteoritic record provides clues regarding which species were once present in one particular protoplanetary disk, our Solar Nebula, and the abundances therein (e.g., Gounelle & Meynet 2012).

A number of studies have quantified the ionization of molecular gas by energetic particles resulting from SLR decay (e.g., Umebayashi & Nakano 1981; Finocchi & Gail 1997; Umebayashi & Nakano 2009). For a disk with an incident CR flux at ISM levels, previous work predicts that ionization by CRs should exceed that of SLRs in regions where the gas surface density  $\Sigma_g < 1000 \text{ g cm}^{-2}$  (Umebayashi & Nakano 1981, 2009). However, under the influence of a wind-reduced CR flux (Paper I), even a modest “present-day” solar wind reduces the CR ionization rate to values rivaling or substantially below that of SLRs ( $\zeta_{\text{CR}} \lesssim 10^{-18} \text{ s}^{-1}$ ) *throughout the disk*. Careful treatment of ionization by SLRs is thus necessary for models of disk chemistry and physics. Furthermore, previous studies of disk ionization by SLRs did not take into account the escape of the decay prod-

ucts, which becomes important when the surface density drops below  $\Sigma_g \lesssim 10 \text{ g cm}^{-2}$ .

In the present paper we develop easy-to-use approximations to implement position-dependent SLR ionization rates in protoplanetary disks,  $\zeta_{\text{SLR}}(r, z)$ , for use in chemical models and/or studies of the magnetorotational instability (Balbus & Hawley 1991). Section 2.1 calculates the ionization rate using a plane-parallel approximation for the radiative transfer, which explicitly includes the escape of decay products from the disk. Although this paper focuses on the dominant ionizing source,  $^{26}\text{Al}$ , we examine the effects of including other SLR species,  $^{60}\text{Fe}$  and  $^{36}\text{Cl}$ , on the estimated ionization rates. Section 2.2 generalizes the calculation to include the effects of dust settling on the ionization rates. Finally, Section 2.3 considers the time evolution of the ionization rates.

## 2. TRANSFER OF SHORT-LIVED RADIONUCLIDE DECAY PRODUCTS

For a given parent SLR, the decay process can result in the emission of  $E \sim 1 \text{ MeV}$  photons, positrons, electrons and  $\alpha$ -particles, whose energy goes into ionization, excitation, and heating of the surrounding gas via secondary electrons (see Umebayashi & Nakano 1981; Dalgarno et al. 1999; Glassgold et al. 2012). Because the SLR mass reservoir in the disk is finite, the half-life  $t_{\text{half}}$ , in addition to the mass/abundance of parent SLRs, is vital, as it sets both the total duration and occurrence rate of the decays. A short half-life results in frequent decays (high ionization rates), but lasts for a potentially negligible fraction of the disk lifetime. From the ionizing secondary electrons, the energy required to create a single ion-pair from  $\text{H}_2$  gas is  $W_{\text{H}_2} = 36 \text{ eV}$ , where only  $\sim 47\%$  of the energy goes into ionization (Dalgarno et al. 1999; Glassgold et al. 2012). As the decay products propagate through the gas disk, the main source of opacity for  $E \sim 1 \text{ MeV}$  photons is Compton scattering and for positrons/electrons is collisional ionization. As a result, the decay products have finite, energy-dependent ranges. The branching ratios, ranges and decay sequences of the SLR parents considered in this work are shown in Table 1. In the following section we compute  $\text{H}_2$  ionization rates; however, these results can be extended to include helium ionization, where  $\zeta_{\text{He}} \approx 0.84\zeta_{\text{H}_2}$  (Umebayashi & Nakano 2009).

The problem of interest is essentially a classical radiative transfer problem where the distribution of emitters follows the refractory material (assuming that most of the radioactive metals are carried by dust grains). Furthermore, we assume that the decay products escape the dust grains from which they are emitted, which is appropriate for dust grain sizes  $a \leq 10 \text{ cm}$  for  $E \sim 1 \text{ MeV}$  photons and  $a \leq 0.1 \text{ cm}$  for positrons (Umebayashi et al. 2013). The absorption is due to energy losses in the gas, and the resulting equation for the frequency-averaged particle/photon intensity,  $I$ , has the general form

$$\hat{s} \cdot \nabla I = \rho_g \left( \frac{100}{f_g} \right) \frac{J}{4\pi} - \rho_g \kappa I, \quad (1)$$

where  $J$  is the emissivity from the production of photons/positrons/electrons due to radioactive decay,  $\kappa$  is the mass absorption coefficient,  $\rho_g$  is the gas density,

TABLE 1  
SELECTED SLR DATA.

Parent SLR $\log_{10}(n_\chi/n_{\text{H}_2})$	$t_{\text{half}}$ (Myr)	Decay Mode	Product (MeV)	$\kappa$ ( $\text{cm}^2/\text{g}$ )
$^{26}\text{Al}$ (-9.378)	0.74	$\beta^+$ 82%	$e^+$ (0.473)	11.76
			$\gamma$ ( $2 \times 0.511$ )	0.148
			$\gamma$ (1.808)	0.080
			$\gamma$ (1.808)	0.080
$^{60}\text{Fe}$ (-10.270)	1.5	E.C. <sup>a</sup> 18%	$e^-$ (0.184)	52.63
			$\gamma$ (0.0586)	0.282
		$\beta^-$ [ $^{60}\text{Co}$ ]	$e^-$ (0.315)	21.74
			$\gamma$ (1.173)	0.101
$^{36}\text{Cl}$ (-10.367)	0.30	$\beta^-$ <sup>c</sup>	$\gamma$ (1.332)	0.094
			$e^-$ (0.7093)	7.541

<sup>a</sup>Electron capture.

<sup>b</sup>The  $^{60}\text{Co}$  half-life is 5.3yr, and therefore we assume it happens instantaneously after the  $^{60}\text{Fe}$  decay event.

<sup>c</sup>There are formally two decay modes:  $\beta^-$  (98%) and  $\beta^+$  (2%). We include only the former in our calculations.

and  $f_g$  is the gas-to-dust mass fraction ( $f_g = 100$  for uniformly distributed gas and dust).

To start, we neglect energy/frequency evolution of the decay product cross sections (see Section 3). To specify  $J$ , we consider decay product ( $k$ ) from a single radioactive species ( $p$ ). If  $E_k$  is the energy of the decay product and  $\omega_p = \log 2/t_{\text{half}}$  is the decay rate, then  $E_k \omega_p$  is the energy generated by  $k$  per second per parent SLR  $p$ . Let  $\chi_p$  be the abundance of the parent species relative to  $\text{H}_2$  and let  $\langle m \rangle = \mu m_{\text{H}}$  denote the mean molecular weight of gas (where  $\mu \approx 2.36$ ). We thus expect the emissivity  $J_k$  to have the form

$$J_k = \frac{E_k \omega_p \chi_p}{\langle m \rangle} \text{ [erg s}^{-1} \text{ g}^{-1} \text{]}. \quad (2)$$

In the regime where all decay products are trapped, the ionization rate per  $\text{H}_2$  is given by the usual expression  $\zeta_{\text{H}_2}^k = E_k \omega_p \chi_p / W_{\text{H}_2} \text{ s}^{-1}$  (e.g., Umebayashi & Nakano 1981). This exercise can be extended over all parent SLRs  $p$ , and decay products  $k$ , within a decay series, thus obtaining:

$$\zeta_{\text{H}_2}^{\text{tot}}(r, z) = \sum_p \sum_k \zeta_{\text{H}_2}^{p,k}(r, z). \quad (3)$$

While the following section provides ionization prescriptions that apply to general disk models, the plots are calculated using our model from Paper I. The gas and dust densities are described by a power-law with an exponential taper at the outer-edge (Andrews et al. 2011) with a total disk gas mass of  $M = 0.04 M_\odot$ . Formally, the vertical dust profile is described by two gaussians for millimeter- (midplane) and micron-sized (atmospheric) grains. For our well-mixed calculation in Section 2.1, we assume instead that the dust follows the gas with a uniform gas-to-dust mass ratio  $f_g = 100$ . For the settled disk discussed in Section 2.2, we compare different methods by which to approximate  $\zeta_{\text{SLR}}$  with more sophisticated dust profiles.

### 2.1. Plane-Parallel Approximation

For disks where the radial variation in density is much slower than variations with height  $z$ , we can treat the disk as essentially an ‘‘infinite slab.’’ We thus carry out

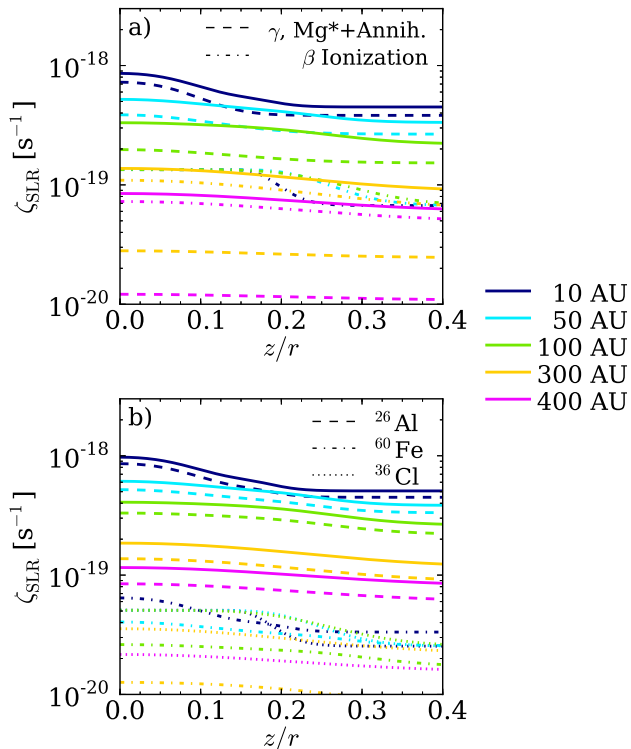


FIG. 1.—  $\text{H}_2$  ionization rate as a function of normalized height ( $z/r$ ) and at specified disk radii (indicated by line color). *Top panel:*  $^{26}\text{Al}$  ionization broken into photon (dashed) and particle processes (dot-dash); solid line represents the total ionization rate. *Bottom panel:* Total ionization from  $^{26}\text{Al}$ ,  $^{60}\text{Fe}$ , and  $^{36}\text{Cl}$ ; individual contributions indicated by dashed, dot-dash, and dotted lines, respectively.

a plane-parallel radiative transfer calculation where intensity  $I$  is a function of height  $z$  above the midplane, and one direction variable. The ray direction is determined by the angle  $\theta$  with respect to the  $z$ -direction, or, equivalently,  $\mu = \cos\theta$ . The validity of this approximation requires that the disk scale height  $H \ll r$ .

In the well-mixed case, the radiative transfer equation (1) has the formal solution:

$$\begin{aligned} I(z, \mu) &= \frac{1}{4\pi} \int_0^\infty \rho J \exp[-\tau(z, \mu; s)] ds \\ &= \frac{1}{4\pi} \int_0^{\tau_\mu(z)} \frac{J}{\kappa} \exp[-\tau(z, \mu; s)] d\tau, \end{aligned} \quad (4)$$

where the optical depth along a ray in the  $\mu$ -direction is

$$\tau(z, \mu; s) = \int_0^s \kappa \rho(s') ds'. \quad (5)$$

Equation (4) allows both the emissivity  $J$  and the opacity  $\kappa$  to vary with position. In many applications, however, these quantities are constant. In general, we want to evaluate the intensity  $I$  at a given height  $z$  and for a given ray direction specified by  $\mu$ . Along the ray, the cylindrical height  $z'$  is given by

$$z' = z - \mu s. \quad (6)$$

Given the optical depth expression (5), and the substi-

tution  $dz' = -\mu ds$ , we can write the optical depth  $\tau_\mu(z)$  in the  $\mu$ -direction in terms of the vertical optical depth  $\tau_\pm$ ,

$$\tau_\mu(z) = -\frac{1}{\mu} \int_z^{\pm\infty} \kappa \rho(z') dz' \equiv \frac{1}{|\mu|} \tau_\pm(z). \quad (7)$$

By separating out the angular dependence from the optical depth, we only need to calculate the  $\tau_\pm$  integrals once for a given location. Accordingly, the specific intensity is given by

$$\begin{aligned} I(z, \mu) &= \frac{J}{4\pi\kappa} (1 - \exp[-\tau_\mu(z)]) \\ &= \frac{J}{4\pi\kappa} \left( 1 - \exp\left[-\frac{1}{|\mu|} \tau_\pm(z)\right] \right). \end{aligned} \quad (8)$$

We integrate (8) over solid angle to determine the total energy density in ionizing decay photons/particles  $\mathcal{E}(z)$ :

$$\begin{aligned} c\mathcal{E}(z) &= \int I(z, \mu) d\Omega = 2\pi \int_{-1}^1 I(z, \mu) d\mu \\ &= 2\pi \int_{-1}^1 \frac{J}{4\pi\kappa} \left( 1 - \exp\left[-\frac{1}{\mu} \tau_\pm(z)\right] \right) d\mu. \end{aligned} \quad (9)$$

Substituting  $t = 1/|\mu|$ , we can evaluate this expression in terms of exponential integrals of order two (Abramowitz & Stegun 1972),

$$\begin{aligned} c\mathcal{E}(z) &= \frac{J}{2\kappa} \left\{ 2 - \int_1^\infty \frac{1}{t^2} \exp[-t\tau_+(z)] dt \right. \\ &\quad \left. - \int_1^\infty \frac{1}{t^2} \exp[-t\tau_-(z)] dt \right\} \\ &= \frac{J}{2\kappa} \{ 2 - E_2[\tau_+(z)] - E_2[\tau_-(z)] \}. \end{aligned} \quad (10)$$

The ionization rate is then given by

$$\zeta_{\text{H}_2}^k(z) = \frac{c\mathcal{E}(z) \langle m \rangle \kappa}{W_{\text{H}_2}} \quad (11)$$

$$= \frac{1}{2} \frac{E_k \omega_p \chi_p}{W_{\text{H}_2}} \{ 2 - E_2[\tau_+(z)] - E_2[\tau_-(z)] \} \quad (12)$$

Equation (12) provides the general solution for the ionization rate due to decay product  $k$  for a well-mixed disk. This expression can be readily evaluated with knowledge of the disk's opacity in the  $z$ -direction. Note that the functions  $E_2(z)$  are standard (e.g., Abramowitz & Stegun 1972, or the Python library *SciPy*).

For a vertically gaussian disk of the form  $\rho_g(z) = \rho_0 \exp[-1/2 (z/H)^2]$ , we can solve exactly for  $\tau_\pm$ ,

$$\tau_\pm(z) = \tau_0 \left\{ 1 \mp \text{erf} \left[ \frac{z}{\sqrt{2}H} \right] \right\}, \quad (13)$$

where we have defined

$$\tau_0 = \kappa \rho_0 H \sqrt{\frac{\pi}{2}} = \frac{\kappa \Sigma_g}{2}. \quad (14)$$

Note that  $\tau_\pm$  must be computed for each type of decay product  $k$  where the decay ranges are provided in Table 1. Nonetheless, Equation (13) allows the ionization rate to

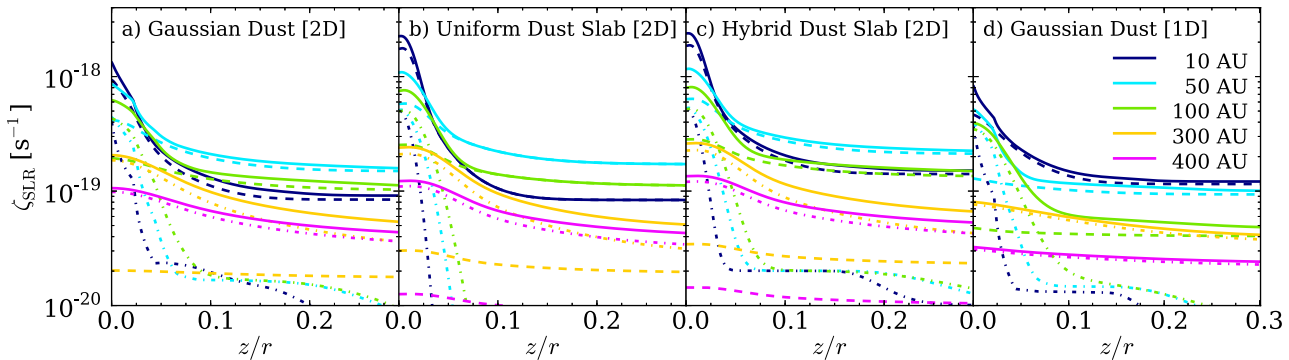


FIG. 2.— Line-styles as indicated in Figure 1 for  $^{26}\text{Al}$  ionization only: a) infinite slab calculation for the original model dust profile; b) infinite slab calculation for a uniform density dust layer in the midplane; c) hybrid model of uniform dust layer combined with a small-grain gaussian distribution; and d) original density profile with decay product escape restricted to the  $z$ -direction.

be calculated – easily and exactly – from Equation (12) at any point  $(r, z)$  in the disk.

Figure 1 presents the results from Equations (12,13) for our standard disk model. Of the various SLR parent bodies,  $^{26}\text{Al}$  dominates the ionization rate  $\zeta_{\text{SLR}}$  at early times, as demonstrated in the bottom panel where we include ionization contributions from  $^{26}\text{Al}$ ,  $^{60}\text{Fe}$ , and  $^{36}\text{Cl}$  decay, which together increase  $\zeta_{\text{SLR}}$  by  $\sim 13\%$ . Among the  $^{26}\text{Al}$  decay products, within  $R < 100$  AU the more energetic  $\gamma$ -rays play the largest role, while outside of this region the more readily stopped positrons carry the ionization (see Figure 1, dashed and dot-dash lines, respectively).

## 2.2. Dust Settling

As dust settles towards the midplane, the sources of emissivity (SLRs in the dust) and the absorbers (gas) are no longer well-mixed. In our settled disk model (Paper I), the large grains have a smaller scale-height  $h$  than the gas and small grains,  $H$ , where both dust reservoirs are described by a gaussian profile and where  $h/H = 0.2$ . This section provides two methods to approximate this more complicated radiative transfer problem.

The original integral for the energy density can be written in the form

$$c\mathcal{E}(z) = \frac{J}{2} \int_{-1}^1 d\mu \int_0^\infty \rho_g(s) \frac{100}{f_g(s)} \exp[-\tau(s)] ds, \quad (15)$$

from which  $\zeta_{\text{SLR}}$  can be directly computed via Equation (11). Using the plane-parallel approximation in conjunction with  $f_g(s) = \rho_g(s)/\rho_d(s)$ , we can solve Equation (15), as was done for the well-mixed case (Section 2.1). In general, this integral must be carried out numerically and is moderately computationally expensive, but it provides an accurate treatment of the problem. We use this numerical result (see Figure 2a) to benchmark the approximations derived below.

### 2.2.1. Uniform Thin Dust Layer

Our first approximation considers the case where the radioactive elements have settled into a thin layer with scale height  $h \ll H$ . We can write the density distribution with the limiting form

$$\rho_d(z) = \Sigma_d \delta(z), \quad (16)$$

where  $\delta(z)$  is the Dirac delta function and  $\Sigma_d = \Sigma_g/100$  is the total dust surface density. With this substitution, the solution to the integral in Equation (4) for a gaussian disk is

$$I(z \gg h; \mu) = \frac{J\Sigma_g}{4\pi\mu} \exp\left[-\frac{\tau_0}{|\mu|} \operatorname{erf}\left(\frac{z}{\sqrt{2}H}\right)\right], \quad (17)$$

which is valid for  $\mu \geq 0$ . In the limit where all SLRs are concentrated at the midplane,  $I = 0$  for  $\mu < 0$ , i.e., nothing is emitted from above. The term in brackets is the optical depth from the midplane to height  $z$  (divided by  $\mu$ ), and can be calculated for a general disk. The corresponding energy density has the form

$$c\mathcal{E}(z) = 2\pi \int_0^1 I(z, \mu) d\mu = \frac{J\Sigma_g}{2} E_1\left[\tau_0 \operatorname{erf}\left(\frac{z}{\sqrt{2}H}\right)\right], \quad (18)$$

where  $E_1(\tau)$  is the exponential integral of order one. In the limit  $\tau \rightarrow 0$ ,  $E_1(\tau) \rightarrow \infty$  as a natural consequence of the  $\delta$ -function. To evaluate the ionization rate near the midplane, we now consider the density distribution to have finite thickness

$$\rho_d(z) = \frac{\Sigma_d}{2\sqrt{2}h} \quad \text{for} \quad |z| \leq \sqrt{2}h, \quad (19)$$

where  $\rho_d(z) = 0$  for  $|z| > \sqrt{2}h$ . With this specification, the specific intensity has the form

$$I(z; \mu) = \frac{J}{4\pi} \frac{\Sigma_g}{2\sqrt{2}h} \int_0^\infty \Theta(z') \exp[-\tau(s)] ds, \quad (20)$$

where  $\Theta(z') = 1$  for  $-\sqrt{2}h \leq z' \leq \sqrt{2}h$  and is zero otherwise. If  $z > \sqrt{2}h$ , then only rays with  $\mu > 0$  result in nonzero  $I$ . Next we define  $t \equiv z'/\sqrt{2}H$  such that

$$\tau(t) = \frac{\tau_0}{|\mu|} \left| \operatorname{erf}\left(\frac{z}{\sqrt{2}H}\right) - \operatorname{erf}(t) \right|. \quad (21)$$

For  $z < \sqrt{2}h$ , the specific intensity becomes

$$I(z < h; \mu > 0) = \frac{J}{4\pi} \frac{\Sigma_g}{\mu} \frac{H}{2h} \int_{-h/H}^{z/H} \exp[-\tau(t)] dt, \quad (22)$$

$$I(z < h; \mu < 0) = \frac{J}{4\pi} \frac{\Sigma_g}{|\mu|} \frac{H}{2h} \int_{z/H}^{h/H} \exp[-\tau(t)] dt. \quad (23)$$

In the limit  $z \rightarrow 0$ , the specific intensity becomes

$$I(z \rightarrow 0, \mu) = \frac{J}{4\pi} \frac{\Sigma_g H}{2h |\mu|} \int_0^{h/H} \exp \left[ -\frac{\tau_0}{|\mu|} \operatorname{erf}(t) \right] dt, \quad (24)$$

where we have used Equation (21). Next we evaluate the specific intensity in the limit  $h \ll H$  where we can approximate  $\operatorname{erf}(t) \approx 2t/\sqrt{\pi}$ , which implies

$$I(z \rightarrow 0, \mu) = \frac{J}{4\pi\kappa} \frac{\sqrt{\pi}H}{2h} \left\{ 1 - \exp \left[ -\frac{\tau_0}{|\mu|} \frac{2h}{\sqrt{\pi}H} \right] \right\}. \quad (25)$$

Defining a “dust-compactness” parameter

$$\lambda \equiv \frac{2h}{\sqrt{\pi}H}, \quad (26)$$

the corresponding energy density at  $z \rightarrow 0$  is given by

$$\begin{aligned} c\mathcal{E}_0 &= \frac{J}{\kappa} \frac{1}{\lambda} \left\{ 1 - \int_1^\infty \frac{\exp[-\tau_0 \lambda x]}{x^2} dx \right\} \\ &= \frac{J}{\kappa} \frac{1}{\lambda} \{1 - E_2[\tau_0 \lambda]\}. \end{aligned} \quad (27)$$

Equations (18) and (27) give the ionization rate  $\zeta_{\text{H}_2}$  in the limits  $z \gg h$  and  $z \rightarrow 0$ , respectively. To provide a continuous expression for  $\zeta_{\text{H}_2}$ , we smoothly connect the two limiting forms,

$$\begin{aligned} \zeta_{\text{H}_2}(z) &= (1 - f(z)) \left\{ \frac{J\Sigma_g}{2} E_1 \left[ \tau_0 \operatorname{erf} \left( \frac{z}{\sqrt{2}H} \right) \right] \right\} \\ &\quad + f(z) \left\{ \frac{J}{\kappa} \frac{1}{\lambda} \{1 - E_2[\tau_0 \lambda]\} \right\}, \end{aligned} \quad (28)$$

where  $f$  is a continuous function, e.g.,  $f = \exp[-z^2/2h^2]$ . In the limit  $\lambda \rightarrow 0$ , Equation (28) provides the solution for a disk model where all of the dust has settled to the midplane. In limit  $\lambda \rightarrow 1$ , we recover the solution for the well-mixed disk (Section 2.1).

Figure 2 (b) shows the ionization rate due to mm-grains (containing 85% of the dust mass) approximated as a thin slab from Equation (28). In panel (c) we combine the results in (b) with the well-mixed calculation for small grains (15% of all dust mass) following Section 2.1, thereby producing a “hybrid” model. At large heights and large radii, the thin-slab solution reproduces the full solution (a) quite well, though slightly overestimates ( $\sim 30 - 60\%$ ) the ionization inside  $R < 50$  AU near the midplane.

### 2.2.2. Bidirectional Escape Approximation

As an alternate approach, we consider only the vertical column of emitters/absorbers, essentially assuming that radiation travels only in the  $z$ -direction. This simplification provides the solution after evaluating only one integral in addition to  $\tau$ , and thus allows us to consider more complex/non-analytic dust and gas distributions. In this “bidirectional escape” approximation, the ioniza-

tion rate has the form

$$\begin{aligned} \zeta_{\text{H}_2}(z) &= \frac{J}{2} \frac{\kappa \langle m \rangle}{W_{\text{H}_2}} \left\{ \int_0^\infty \rho_g(z) \left( \frac{100}{f_g(z)} \right) \exp[-\tau(z)] dz \right. \\ &\quad \left. + \int_0^{-\infty} \rho_g(z) \left( \frac{100}{f_g(z)} \right) \exp[-\tau(z)] dz \right\}. \end{aligned} \quad (29)$$

where  $\tau_\pm$  are given by Equation (13). Although this approximation is somewhat crude, the solution can be readily evaluated via numerical integration, where the emissivity  $J$  is given by Equation (2). Figure 2 (d) compares this bidirectional approximation to the plane-parallel calculation for the same dust density profile. In general, the bidirectional calculation underestimates the ionization rate by a factor of  $\sim 1.5$ , with the discrepancy growing to a factor of  $\sim 2$  for  $R \geq 300$  AU.

### 2.3. Time Dependence

Technically, the abundances of the SLRs evolve with time, with half-lives  $t_{\text{half}} \sim 1$  Myr, comparable to disk evolution timescales. We have calculated the ionization rates for the unsettled disk at  $t = 1, 5$  and 10 Myr, to compare with the  $t = 0$  calculations from Section 2 (Figure 1); these results are presented in Figure 3. At early times,  $^{26}\text{Al}$  and  $^{36}\text{Cl}$  are the dominant ionizing agents; after  $\sim 5$  Myr, however, the longer-lived though less abundant  $^{60}\text{Fe}$  determines the ionization rate  $\zeta_{\text{SLR}}$ . At even longer times, long-lived radionuclides such as  $^{40}\text{K}$  ( $t_{\text{half}} \sim 1.28$  Gyr; Umebayashi et al. 2013) provide the largest contribution. However, because the ionization rate is inversely proportional to  $t_{\text{half}}$ , long-lived radionuclides only produce ionization rates of order  $\zeta_{\text{H}_2} \lesssim 10^{-22} \text{ s}^{-1}$ .

Figure 4 plots the ionization rate  $\zeta_{\text{SLR}}$  calculated at the disk midplane ( $z = 0$ ) versus vertical disk surface density at several times. We have fitted power-laws (shown in gray in Figure 4) to the ionization rates from all three SLR species to facilitate their use. For the well-mixed disk, the rate  $\zeta_{\text{H}_2}$ , as a function of disk surface density and time, is given by

$$\zeta_{\text{H}_2}(r) = (2.5 \times 10^{-19} \text{ s}^{-1}) \left( \frac{1}{2} \right)^{1.04t} \left( \frac{\Sigma(r)}{\text{g cm}^{-2}} \right)^{0.27}, \quad (30)$$

where time,  $t$ , is given in Myr.

## 3. DISCUSSION

This work has made two simplifying assumptions that warrant further consideration. First, we have used a single opacity to simplify the calculations. In reality, the photons and particles will have their energies degraded as they collide with the gas. For Compton-scattered photons, the change in  $\gamma$ -ray energy for  $E_\gamma < m_e c^2$  is approximately  $\Delta E \propto E_\gamma^2$  (Rybicki & Lightman 1979). This energy degradation results in an energy spectrum of the form  $I(E_\gamma) \approx E_\gamma dN/dE \approx E_\gamma/\Delta E \propto 1/E_\gamma$ , from which we may compute a weighted opacity for photons that lose all of their energy through scattering in the disk,

$$\langle \kappa \rangle \equiv \frac{\int_0^{E_i} \kappa(E_\gamma) I dE}{\int_0^{E_i} I dE}. \quad (31)$$

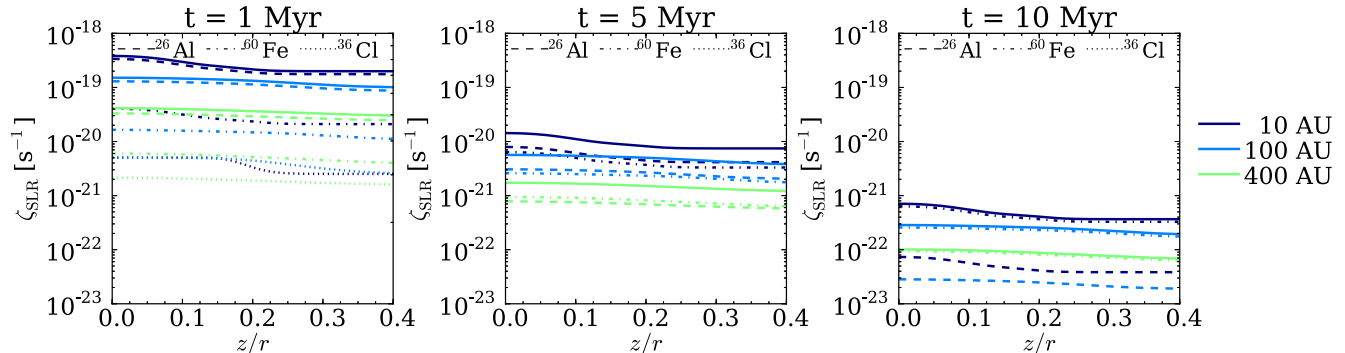


FIG. 3.— Same as Figure 1, at the indicated time after  $t = 0$  such that the ionizing reservoir has been partially exhausted. For  $t < 5$  Myr, the ionization rate is set by  $^{26}\text{Al}$ -decay. At later times (right,  $t = 10$  Myr) the longer-lived  $^{60}\text{Fe}$  provides the ionization, although at a reduced rate due to its lower abundance and longer decay time.

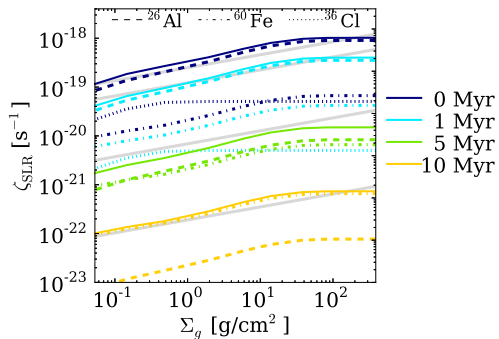


FIG. 4.— Ionization rate per  $\text{H}_2$  in the midplane as a function of disk surface density at the indicated times. We fit these results using a simple power-law versus surface density, normalized to a time-dependent constant (gray lines), see Equation (30).

At sufficiently low energies, below  $E_\gamma < 30$  keV, the dominant absorption mechanism becomes photoabsorption, at which point the photon has lost nearly all of its initial energy  $E_i \sim 1$  MeV. The Compton-weighted opacity for a 1.808 MeV photon is  $\langle \kappa \rangle \sim 0.19 \text{ cm}^2 \text{ g}^{-1}$ , larger than its initial cross section,  $\kappa_i \sim 0.08 \text{ cm}^2 \text{ g}^{-1}$ , which increases the derived ionization rate by factors of 4% (12%) at  $r = 10$  AU (400 AU).

Another major simplification comes from our treatment of the positrons in  $^{26}\text{Al}$  decay. Currently we assume that all energetic particles are emitted locally and can then escape. According to Umebayashi et al. (2013), the positron will first lose its energy to primarily collisional ionization until it comes to rest, at which point it will annihilate with an electron and produce two 0.511 MeV  $\gamma$ -rays. However, the cross section for absorption of the  $\gamma$ -rays is less than that of the original positrons. For disk regions where positrons escape in our simplified treatment, these  $\gamma$ -rays escape even more readily, and thus make smaller contributions to the ionization rate.

#### 4. CONCLUSION

This paper carries out radiative transfer calculations for the decay products of short-lived radionuclides in

circumstellar disks. These SLRs provide an important contribution to the ionization rates, which in turn affect disk chemistry and physics. We provide simple analytic expressions for the ionization rates due to SLR decay. For well-mixed disks, the ionization rate  $\zeta_{\text{SLR}}(r, z)$  can be found analytically and is given by Equation (12). The radial dependence is controlled by the surface density profile, which determines the optical depths through Equations (13) and (14). Complications arise as disks evolve, including dust settling and a decrease in the SLR abundances. We provide two approximations for disks with settled dust layers: The first treatment considers the dust as a thin uniform layer; the ionization rate is given by Equation (28), where the dust-compactness parameter  $\lambda$  determines the degree of settling (Equation (26)). This approximation scheme is accurate to tens of percent, and becomes exact for a well-mixed disk. For completeness, we develop a simpler approximation that considers radiation propagation in the vertical directions only (Section 2.2.2), as is commonly done for calculations of CR ionization rates. Finally, we provide a fit to the midplane ionization rates as a function of surface density and time (Equation (30)). While this function can be applied over the entire vertical structure, it formally overestimates  $\zeta_{\text{H}_2}^{\text{SLR}}$  at the disk surface. In this regime, however, other ionization sources (e.g., stellar X-ray photoionization of  $\text{H}_2$ ) will dominate, so that our approximation remains satisfactory.

A full treatment of this problem requires Monte Carlo or other numerical methods, including energy losses, angle-dependent scattering, energy-dependent radiative transfer, and more sophisticated density distributions. Although these generalizations should be incorporated in future work, the analytic expressions derived herein provide useful and accurate estimates for the ionization rates due to SLR decay, and can thus be used in a wide variety of physical and chemical disk models.

This work was supported by NSF grant AST-1008800.

#### REFERENCES

- Abramowitz, M. & Stegun, I. A. 1972, Handbook of Mathematical Functions  
 Adams, F. C. 2010, ARA&A, 48, 47  
 Andrews, S. M., Wilner, D. J., Espaillat, C., Hughes, A. M., Dullemond, C. P., McClure, M. K., Qi, C., & Brown, J. M. 2011, ApJ, 732, 42  
 Arould, M., Paulus, G., & Meynet, G. 1997, A&A, 321, 452

- Balbus, S. A. & Hawley, J. F. 1991, *ApJ*, 376, 214
- Cameron, A. G. W. & Truran, J. W. 1977, *Icarus*, 30, 447
- Cleeves, L. I., Adams, F. C., & Bergin, E. A. 2013, *ApJ*, 772, 5
- Dalgarno, A., Yan, M., & Liu, W. 1999, *ApJS*, 125, 237
- Diehl, R., Halloin, H., Kretschmer, K., Lichti, G. G., Schönfelder, V., Strong, A. W., von Kienlin, A., Wang, W., Jean, P., Knödseder, J., Roques, J.-P., Weidenspointner, G., Schanne, S., Hartmann, D. H., Winkler, C., & Wunderer, C. 2006, *Nature*, 439, 45
- Finocchi, F. & Gail, H.-P. 1997, *A&A*, 327, 825
- Gaidos, E., Krot, A. N., Williams, J. P., & Raymond, S. N. 2009, *ApJ*, 696, 1854
- Glassgold, A. E., Galli, D., & Padovani, M. 2012, *ApJ*, 756, 157
- Glassgold, A. E., Najita, J., & Igea, J. 1997, *ApJ*, 480, 344
- Glassgold, A. E. & Najita, J. R. 2001, in *Astronomical Society of the Pacific Conference Series*, Vol. 244, *Young Stars Near Earth: Progress and Prospects*, ed. R. Jayawardhana & T. Greene, 251
- Gounelle, M. & Meynet, G. 2012, *A&A*, 545, A4
- Lee, T., Shu, F. H., Shang, H., Glassgold, A. E., & Rehm, K. E. 1998, *ApJ*, 506, 898
- MacPherson, G. J., Davis, A. M., & Zinner, E. K. 1995, *Meteoritics*, 30, 365
- Rybicki, G. B. & Lightman, A. P. 1979, *Radiative processes in astrophysics*
- Shang, H., Shu, F. H., Lee, T., & Glassgold, A. E. 2000, *Space Sci. Rev.*, 92, 153
- Umebayashi, T., Katsuma, N., & Nomura, H. 2013, *ApJ*, 764, 104
- Umebayashi, T. & Nakano, T. 1981, *PASJ*, 33, 617
- . 2009, *ApJ*, 690, 69
- Walsh, C., Nomura, H., Millar, T. J., & Aikawa, Y. 2012, *ApJ*, 747, 114